

## Detecting Interstellar Objects Through Stellar Occultations

AMIR SIRAJ<sup>1</sup> AND ABRAHAM LOEB<sup>1</sup><sup>1</sup> Department of Astronomy, Harvard University, 60 Garden Street, Cambridge, MA 02138, USA

## ABSTRACT

Stellar occultations have been used to search for Kuiper Belt and Oort Cloud objects. We propose a search for interstellar objects based on the characteristic durations ( $\sim 0.1$ s) of their stellar occultation signals and high inclination relative to the ecliptic plane. An all-sky monitoring program of  $\sim 2 \times 10^7$  stars with an R-band magnitude of 14 using 1-m telescopes with 0.1 s cadences, is predicted to discover  $\gtrsim 5$  interstellar objects per year.

*Keywords:* Minor planets, asteroids: general – meteorites, meteors, meteoroids

## 1. INTRODUCTION

‘Oumuamua was the first interstellar object (ISO) reported in the Solar System (Meech et al. 2017; Micheli et al. 2018). Follow-up studies of ‘Oumuamua were conducted to better understand its origin and composition (Bannister et al. 2017; Gaidos et al. 2017; Jewitt et al. 2017; Mamajek 2017; Ye et al. 2017; Bolin et al. 2017; Fitzsimmons et al. 2018; Trilling et al. 2018; Bialy & Loeb 2018; Hoang et al. 2018; Siraj & Loeb 2019a,b; Seligman et al. 2019). ‘Oumuamua’s size was estimated to be  $\lesssim 200$  m, based on Spitzer Space Telescope constraints on its infrared emission given its expected surface temperature based on its orbit (Trilling et al. 2018).

In addition to ‘Oumuamua, CNEOS 2014-01-08 (Siraj & Loeb 2019a) was tentatively the first interstellar meteor discovered larger than dust, and 2I/Borisov (Guzik et al. 2019) was the first confirmed interstellar comet.

Transient diffraction patterns caused by the occultation of a distant star due to an intervening small body have been used to search for Kuiper Belt objects (KBOs) and Oort Cloud objects (OCOs) in the Solar System (Bailey 1976; Dyson 1992; Roques & Moncuquet 2000; Nihei et al. 2007; Schlichting et al. 2009, 2012; Arimatsu et al. 2019). Here, we propose an analogous search for interstellar objects (ISOs), flagged by their unusual inclinations and unique kinematics leading a distribution of characteristic distribution of durations, the peak of which lies between that of Kuiper belt objects and that of Oort cloud objects.

amir.siraj@cfa.harvard.edu, aloeb@cfa.harvard.edu

The data from such a search would calibrate population parameters for ISOs crucial for constraining formation theories of exoplanetary systems (Duncan et al. 1987; Charnoz & Morbidelli 2003; Veras et al. 2011, 2014; Pfalzner et al. 2015; Do et al. 2018; Raymond et al. 2018; Hands et al. 2019; Pfalzner & Bannister 2019; Siraj & Loeb 2019d). Below we derive the physical characteristics and rate of the expected ISO occultation events.

## 2. THEORY

The measured intensity at wavelength  $\lambda$  from a diffraction pattern created by a spherical object of radius  $R_L$  at a distance  $D_L$  is,

$$I_\rho(t) = \begin{cases} U_0^2(\rho, t/t_F) + U_1^2(\rho, t/t_F), & t/t_F \leq \rho, \\ 1 + U_1^2(\rho, t/t_F) + U_2^2(\rho, t/t_F) \\ -2U_1(\rho, t/t_F) \sin \frac{\pi}{2}(\rho^2 + (t/t_F)^2) \\ +2U_2(\rho, t/t_F) \cos \frac{\pi}{2}(\rho^2 + (t/t_F)^2), & t/t_F \geq \rho, \end{cases} \quad (1)$$

where  $\rho = (R_L/F)$  is the radius of the object in units of the Fresnel scale  $F = \sqrt{\lambda D_L/2}$ , and  $t_F$  is the Fresnel scale crossing time for the object (Nihei et al. 2007; Roques et al. 1987). For a transverse speed,  $v_\perp$ , at a distance  $D_L$ , the Fresnel time is  $t_F = 0.12s (D_L/20 \text{ AU})^{1/2} (v_\perp/10 \text{ km s}^{-1})^{-1} (\lambda/\mu\text{m})^{1/2}$  and the Fresnel scale is  $F = 1.2\text{km} (D_L/20 \text{ AU})^{1/2} (\lambda/\mu\text{m})^{1/2}$ . The Lommel functions are defined as,

$$U_n(\mu, \nu) = \sum_{k=0}^{\infty} (-1)^k \left(\frac{\mu}{\nu}\right)^{n+2k} J_{n+2k}(\pi\mu\nu), \quad (2)$$

where  $J_n$  is a Bessel function of order  $n$ . With regard to the impact parameter  $b$ , we assume  $b = 0$  for simplicity.

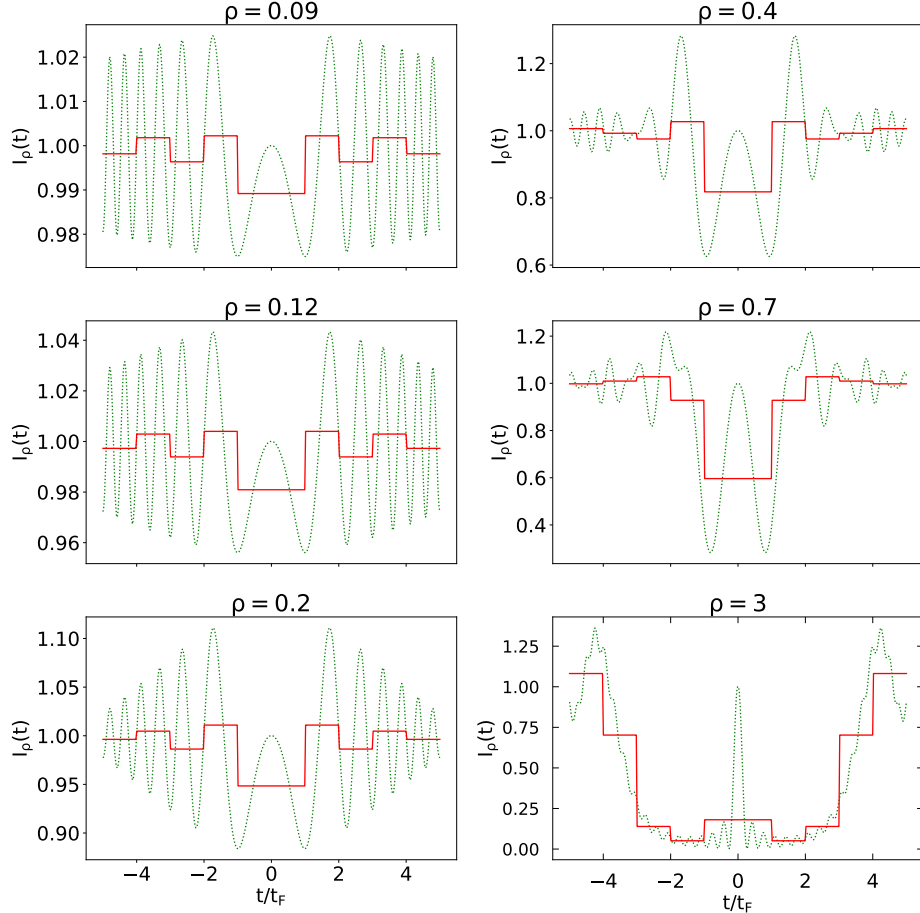


**Figure 1.** Occultation lightcurves for the values of  $\rho_{min}$  (ratio of ISO radius to the Fresnel scale) in Table 1 (dotted green lines), and sampled lightcurves at temporal resolution,  $t_F$  (solid red lines). For a transverse speed  $v_{\perp}$  at a distance  $D_L$ , the time unit,  $t_F = 0.1s (D_L/20 \text{ AU})^{1/2} (v_{\perp}/10 \text{ km s}^{-1})^{-1}$ .

Figure 1 shows lightcurves for different values of  $\rho$ , as well as lightcurves sampled as at a spatial resolution of  $F$ .

For a solar-type star with an R-magnitude of 14, the flux of R-band photons at Earth is  $\sim 4.4 \times 10^4 \text{ m}^{-2} \text{ s}^{-1}$ . For an intensity dip caused by an occultation event, a signal to Poisson noise ratio of  $\gtrsim 5$  for a telescope with  $1 \text{ m}^2$  collecting area with a temporal resolution of  $t_f$  would require the intensity dip to be  $\gtrsim 2\%$ , corresponding to  $\rho \gtrsim 0.12$ . The appropriate values of  $\rho_{min}$  as a function of magnitude are listed in Table 1.

In addition to  $\rho \geq \rho_{min}$  for a strong signal, we also require the occulting object to subtend a larger angular size on the sky than the star to avoid dilution of the signal by the finite source size. We adopt the conservative condition  $R_L \leq 10 \text{ km}$  for ISOs. Given a star of radius

$R_S$  and distance  $R_L$ , the three conditions for an ISO occultation event are expressed as follows:

$$R_L > \rho_{min} \sqrt{\frac{\lambda D_L}{2}} , \quad (3)$$

$$\frac{R_L}{D_L} > \frac{R_S}{D_S} , \quad (4)$$

$$R_L < 10 \text{ km} . \quad (5)$$

Figure 2 illustrates a parameter space in which all three conditions are satisfied.

We approximate the cumulative number density of ISOs as a power law with exponent -3.3, calibrated by the number density ( $n_O \sim 0.2 \text{ AU}^{-3}$ ) of ‘Oumuamua size ( $R_O \sim 100 \text{ m}$ ) objects (Siraj & Loeb 2019c; Do et al. 2018; Landgraf et al. 2000).

We adopt the three-dimensional velocity dispersion of stars in the thin disk of the Milky Way as a proxy for the kinematics of ISOs, each corresponding to the

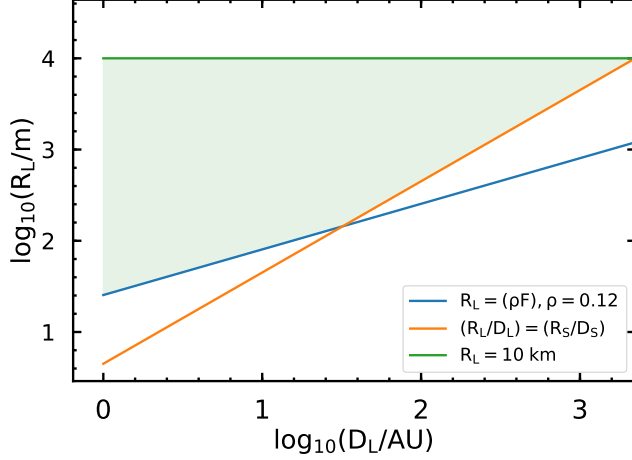


**Figure 2.** Parameter space in which conditions (3), (4), and (5), are satisfied for a  $R = 14$  solar-type star.  $R_S \sim R_\odot$  and  $D_S \sim 740$  pc for an  $R = 14$  solar-type star.

**Table 1.** Background photon flux, maximum dip in intensity, and minimum value of  $\rho$  for occultation events with solar-type background stars, assuming a  $1 \text{ m}^2$  collecting area and a temporal resolution of  $t_f$ .

R Magnitude	R-Band Photon Flux ( $\text{m}^{-2}\text{s}^{-1}$ )	$\Delta I_{\min}$ (%)	$\rho_{\min}$
12	$2.8 \times 10^5$	1	0.09
14	$4.4 \times 10^4$	2	0.12
16	$6.9 \times 10^3$	6	0.2
18	$1.1 \times 10^3$	16	0.4
20	$1.7 \times 10^2$	38	0.7
22	28	95	3

standard deviation of a Gaussian distribution about the local standard of rest (LSR):  $\sigma_x = 35 \text{ km s}^{-1}$ ,  $\sigma_y = 25 \text{ km s}^{-1}$ ,  $\sigma_z = 25 \text{ km s}^{-1}$  (Bland-Hawthorn & Gerhard 2016). The resulting distribution of observed transit speeds (once the motion of the Earth is subtracted) has a mean value of  $\bar{v}_{\text{obs}} \sim 40 \text{ km s}^{-1}$ .

The rate of occultations per star is given by,

$$\begin{aligned} \dot{N}_{O,\star} = & \\ & 2\pi \int_{1 \text{ AU}}^{L_1} n_O \left[ \left( \frac{\rho_{\min} \sqrt{\lambda D_L/2}}{R_O} \right)^{-3.3} - \left( \frac{R_{\max}}{R_O} \right)^{-3.3} \right] \\ & \left( \frac{\bar{v}_{\text{obs}} D_L R_S}{D_S} \right) \text{d}D_L + \\ & 2\pi \int_{L_1}^{L_2} n_O \left[ \left( \frac{R_S D_L}{D_S R_O} \right)^{-3.3} - \left( \frac{R_{\max}}{R_O} \right)^{-3.3} \right] \\ & \left( \frac{\bar{v}_{\text{obs}} D_L R_S}{D_S} \right) \text{d}D_L, \end{aligned} \quad (6)$$

where the limits of the integrals,  $L_1$  and  $L_2$ , are defined as follows:

$$L_1 = \begin{cases} \frac{\rho_{\min}^2 \lambda D_S^2}{2R_S^2}, & \frac{\rho_{\min}^2 \lambda D_S^2}{2R_S^2} \leq \frac{R_{\max} D_S}{R_S} \\ \frac{2R_{\max}^2}{\rho_{\min}^2 \lambda}, & \frac{\rho_{\min}^2 \lambda D_S^2}{2R_S^2} \geq \frac{R_{\max} D_S}{R_S} \end{cases}, \quad (7)$$

$$L_2 = \begin{cases} \frac{R_{\max} D_S}{R_S}, & \frac{\rho_{\min}^2 \lambda D_S^2}{2R_S^2} \leq \frac{R_{\max} D_S}{R_S} \\ 0, & \frac{\rho_{\min}^2 \lambda D_S^2}{2R_S^2} \geq \frac{R_{\max} D_S}{R_S} \end{cases}. \quad (8)$$

The resulting ISO occultation rate per star as a function of magnitude peaks at  $R = 14$ , corresponding to  $\sim 0.3 \text{ Myr}^{-1}$ , and is shown in Figure 3.

To determine how easily discernable ISO, KBO, and OCO occultation signatures are from each other, and to understand the distribution of timescales on which ISO occultations occur, we numerically simulated the distribution of expected Fresnel distance crossing times for each population, assuming a  $R = 14$  solar-type star.

We draw distances from the distribution  $P(D_L) \propto D_L^2$  with bounds of 1 AU to  $(R_{\max} D_S / R_S)$  for ISOs, bounds of 30 to 50 AU for KBOs, and bounds of  $2 \times 10^3$  to  $10^5$  AU for OCOs. We draw velocities from the aforementioned kinematics for ISOs; we compute the orbital speed corresponding the distance for KBOs and for OCOs. We do not consider gravitational focusing and acceleration by the Sun for ISOs as these effects would only be significant at  $D_L \lesssim 1$  AU. We sample random points in the Earth's orbit to obtain the motion of the observer relative to the object. We draw sizes for each population from a power law distribution with index  $\sim -3$ , with the appropriate bounds for each population. If conditions (4) and (5) are satisfied, we compute

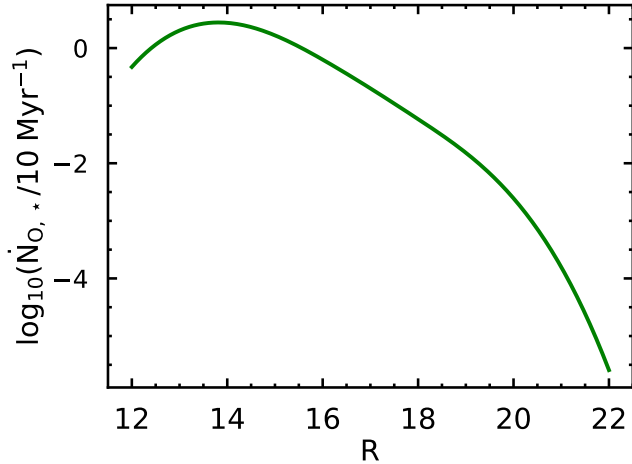


**Figure 3.** ISO occultation rate per star as a function of R magnitude for solar-type stars.

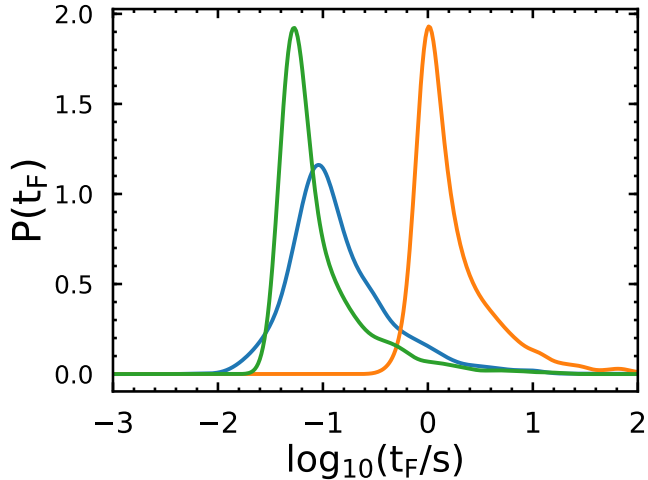


**Figure 4.** Expected probability distribution of Fresnel crossing times during stellar occultations observed from Earth for ISOs (blue), KBOs (green), and OCOs (orange), for a  $R = 14$  solar-type star.

the Fresnel distance crossing time,  $t_F = (F/v_\perp)$ . Otherwise, we re-draw distance and size. The resulting distributions of  $t_F$  are shown in Figure 4. ISO occultation events have an even distribution with distance between 1 AU and  $\sim 10^3$  AU. We find that the timescales for ISO and OCO occultation events are distinct. The ISO timescale distribution peaks at  $t_F = 0.1$  s, and a survey can avoid KBOs by pointing away from the plane of the ecliptic.

### 3. CONCLUSIONS

There are  $\sim 2 \times 10^7$  stars in a 1-magnitude bin centered around  $R = 14$  (Anders et al. 2019). An all-sky

network of 1-m telescopes continuously monitoring all  $R = 14$  stars with a time resolutions of 0.1 s should yield a discovery rate of  $\gtrsim 5$  interstellar objects per year. This would be an improvement by an order of magnitude on the current discovery rate of an ISO every few years. Our method supplements direct detection through reflected sunlight but nearby events could benefit from both methods of detection. By measuring each occultation in two or three colors, the radius and distance of the occulting object can be constrained (Dyson 1992).

The data from such a survey would provide invaluable new information on the size distribution, composition, and possible origin of ISOs. Such information

would be particularly valuable given the puzzle of the first two confirmed interstellar objects, ‘Oumuamua and Borisov, having such different physical characteristics (Meech et al. 2017; Guzik et al. 2019), and given the

high implied abundance of ISOs relative to previous predictions (Moro-Martin 2009).

## ACKNOWLEDGEMENTS

This work was supported in part by a grant from the Breakthrough Prize Foundation.

## REFERENCES

Anders F., et al., 2019, *Astronomy & Astrophysics*, 628, A94

Arimatsu K., 2019, *Nature Astronomy*, 3, 301

Bailey M., et al., 1976, *Nature*, 259, 290

Bannister M. T., et al., 2017, *The Astrophysical Journal*, 851, L38

Bialy S., Loeb A., 2018, *The Astrophysical Journal*, 868, L1

Bland-Hawthorn J., Gerhard O., 2016, *Annual Review of Astronomy and Astrophysics*, 54, 529

Bolin B. T., et al., 2017, *The Astrophysical Journal Letters*, Volume 852, Issue 1, article id. L2, 10 pp. (2018)., 852

Charnoz S., Morbidelli A., 2003, *Icarus*, 166, 141

Do, A., Tucker, M. A., Tonry, J. 2018, *The Astrophysical Journal*, 855, L10

Duncan, M., Quinn, T., Tremaine, S. 1987, *The Astronomical Journal*, 94, 1330

Dyson M., 1992, Royal Astronomical Society, Quarterly Journal, 33, 45

Engelhardt T., et al., 2017, *The Astronomical Journal*, 153, 133

Fitzsimmons A., et al., 2018, *Nature Astronomy*, 2, 133

Gaidos E., Williams J., Kraus A., 2017, *Research Notes of the AAS*, 1, 13

Guzik., et al., 2019, Interstellar comet C/2019 Q4 (Borisov). ([arXiv:1909.05851](https://arxiv.org/abs/1909.05851))

Hoang T., Loeb A., Lazarian A., Cho J., 2018, *The Astrophysical Journal*, 860(1), 42

Hands T. O., et al., 2019, *MNRAS*

Jewitt D., Luu J., Rajagopal J., Kotulla R., Ridgway S., Liu W., Augusteijn T., 2017, *The Astrophysical Journal*, 850, L36

Landgraf, M., Baggaley, W. J., Grun, E., Kruger, H., Linkert, G., 2000, *J. Geophys. Res.*, 105, 10343

Mamajek E., 2017, *Research Notes of the AAS*, 1, 21

Meech K. J., et al., 2017, *Nature*, 552, 378

Micheli M., et al., 2018, *Nature*, 559, 223

Moro-Martin A., et al., 2009, *The Astrophysical Journal*, 704, 733

Moro-Martin A., et al., 2019, *The Astrophysical Journal*, 157, 86

Nihei M., et al., 2007, *The Astronomical Journal*, 134, 1596

Pfalzner S., et al., 2015, *Phys S*, 794, 147

Pfalzner S., Bannister M. T., 2019, *The Astrophysical Journal*, 874, L34

Raymond S. N., et al., 2018, *MNRAS*, 476, 3031

Roques F., Moncuquet M., 2000, *Icarus*, 147, 530

Roques F., et al., 1987, *Astronomical Journal*, 93, 1549

Schlichting H. E., 2009, *Nature*, 462, 895

Schlichting H. E., 2012, *The Astrophysical Journal*, 761, 150

Seligman D., Laughlin G., Batygin K., 2019, *The Astrophysical Journal Letters*, 872(1), L10

Siraj A. & Loeb A., 2019a, *The Astrophysical Journal*, 872(1), L10

Siraj A. & Loeb A., 2019b, *Research Notes of the American Astronomical Society*, 3(1), 15

Siraj A. & Loeb A., 2019c, Discovery of a Meteor of Interstellar Origin. ([arXiv:1904.07224](https://arxiv.org/abs/1904.07224))

Siraj A. & Loeb A., 2019d, Probing Extrasolar Planetary Systems with Interstellar Meteors. ([arXiv:1906.03270](https://arxiv.org/abs/1906.03270))

Trilling, D., et al., 2018, *The Astronomical Journal*, 156, 261.

Veras D., et al., 2011, *MNRAS*, 417, 2104

Veras D., et al., 2014, *MNRAS*, 437, 1127

Ye Q.-Z., Zhang Q., Kelley M. S. P., Brown P. G., 2017, *The Astrophysical Journal*, 851, L5